Supporting Information

Bifunctional Polymer-of-Intrinsic-Microporosity Membrane for Flexible Li/Na-H_2O_2 Batteries with Hybrid Electrolytes

Yunfeng Zhao,[a] Xiaorong Ma,[a] Pengli Li,[a] Yang Lv,[a] Jianfeng Huang,[b] Haixia Zhang,[a] Yongli Shen,[a] Qibo Deng,[a] Xizheng Liu,[a,*] Yi Ding,[a] Yu Han[c,*]

[a] Tianjin Key Laboratory of Advanced Functional Porous Materials, Institute for New-Energy Materials and Low-Carbon Technologies, School of Materials Science and Engineering, Tianjin University of Technology, Tianjin 300384, P. R. China

[b] Multi-scale Porous Materials Center, Institute of Advanced Interdisciplinary Studies & College of Materials Science and Engineering, Chongqing University, Chongqing 400044, P. R. China

[c] Advanced Membranes and Porous Materials Center, King Abdullah University of Science and Technology, Thuwal 23955-6900, Kingdom of Saudi Arabia

AUTHOR INFORMATION

Corresponding Author

xzliu@tjut.edu.cn (X Liu), yu.han@kaust.edu.sa (Y. Han)

Chemicals and characterizations. Sodium hydroxide (NaOH, >98%), chloroform (>99%), potassium carbonate (K_2CO_3, 99.99%), N,N-dimethylacetamide (DMAc, 99.5%), tetrahydrofuran (THF, 99.5%), ethanol (99.7%), and methanol (99.5%) were purchased from Aladdin and used as received. 5,5',6,6'-Tetrahydroxy-3,3,3',3'-tetramethyl-1,1'-spirobisindane (TTSBI, Alfa) was purified through recrystallization in methanol. Tetrafluoroterephthalonitrile (DCTB, Alfa) was purified via vacuum sublimation at 120 °C. Infrared (IR) spectra were recorded using a Frontier Mid-IR Fourier transform IR spectrometer. The pore size was measured through CO_2 adsorption under 273 K with an Autosorb-iQ-MP analyzer. Thermogravimetric analysis was performed at a rate of 10 °C/min in N_2 and air using a TG 209 F3 analyzer (Perlin Elmer). X-ray photoelectron spectroscopy analyses were performed using a Thermo Scientific Escalab 250Xi. Scanning electron microscopy was performed on an FEI Verios 460L. Tensile and puncture tests were performed at a quasi-static speed of 1 mm/min at room temperature on an universal tensile machine (XJ 830, Shanghai Xiangjie).

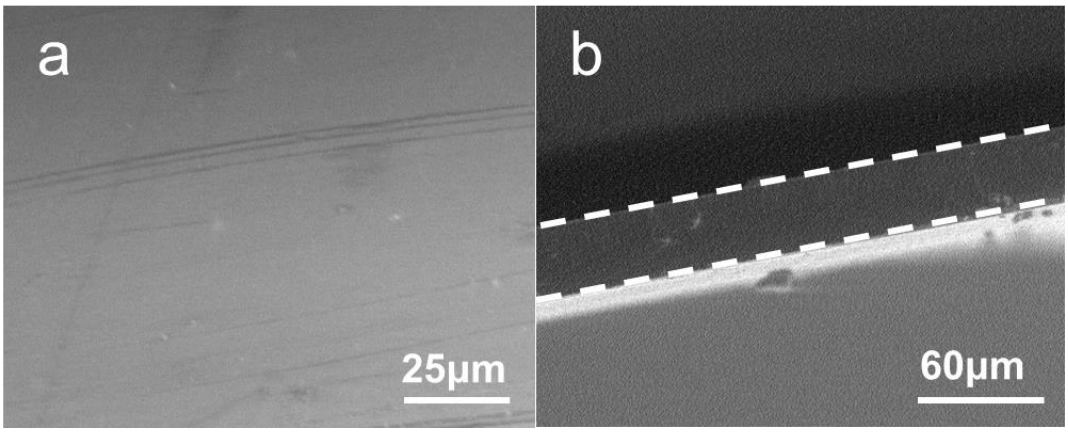

Fig. S1 SEM images of the surface (a) and the cross section (b) of hydrolyzed PIM-1 membrane without the formation of macropores by adding LiTFSI salt.

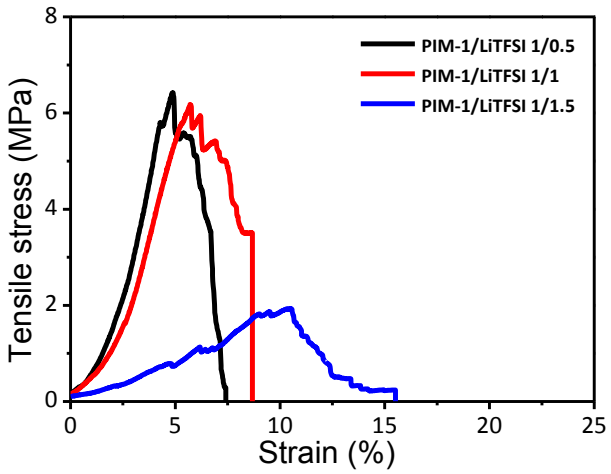

Fig. S2 Tensile stress curves of PIM-1-COOLi membrane prepared with different Li salt compositions.

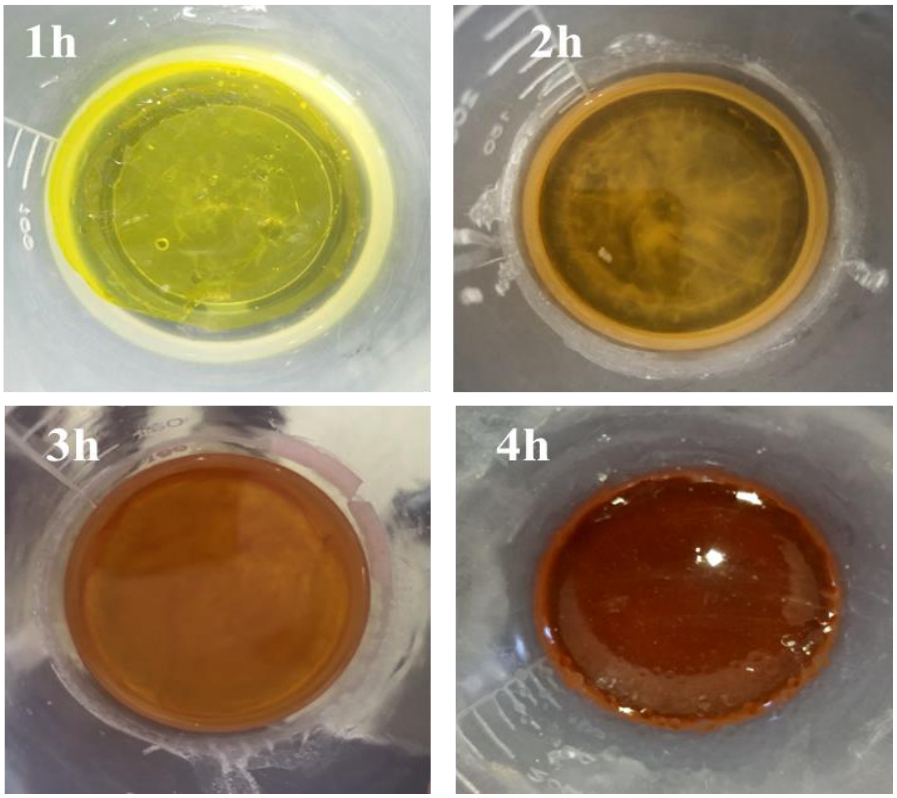

Fig. S3 Photo pictures of the PIM-1 membrane at different stages during the hydrolysis process.

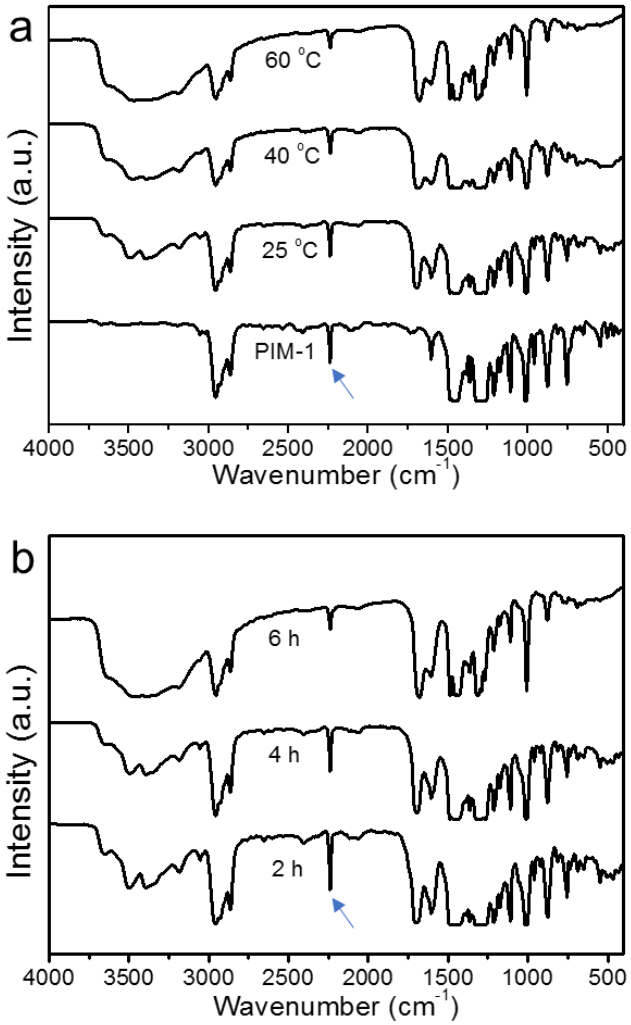

Fig. S4 FTIR spectra of PIM-1-COOLi membranes hydrolyzed under different conditions: (a) at different temperatures for 6 h; (b) at 60 °C for different times.

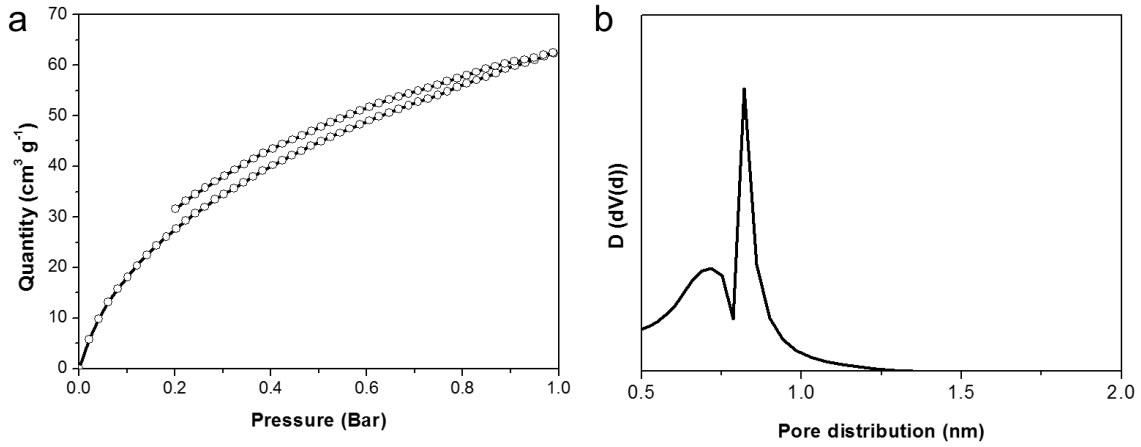

Fig. S5 The CO_2 adsorption-desorption isotherm at 273 K (a) and the derived pore size distribution profile (b) of the PIM-1-COOLi membrane.

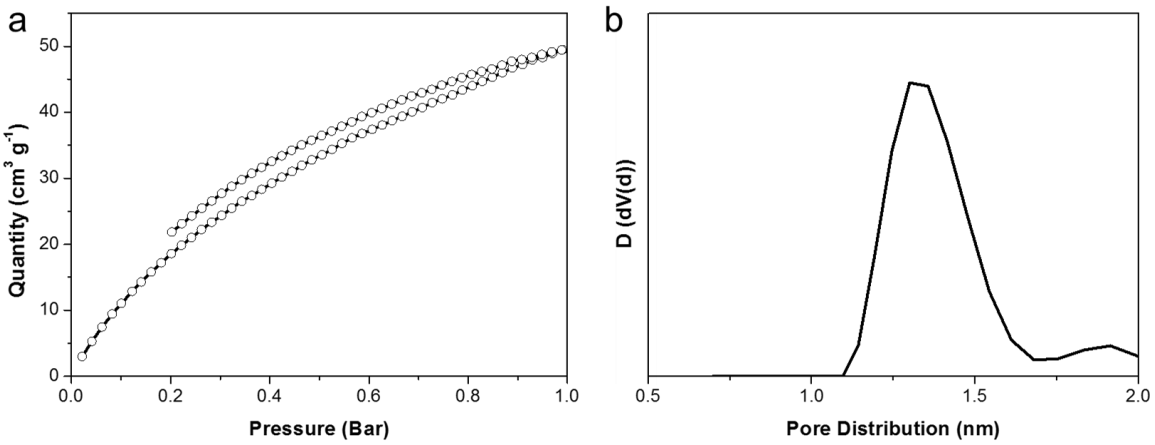

Fig. S6 The CO_2 adsorption-desorption isotherm at 273 K (a) and the derived pore size distribution profile (b) of the PIM membrane.

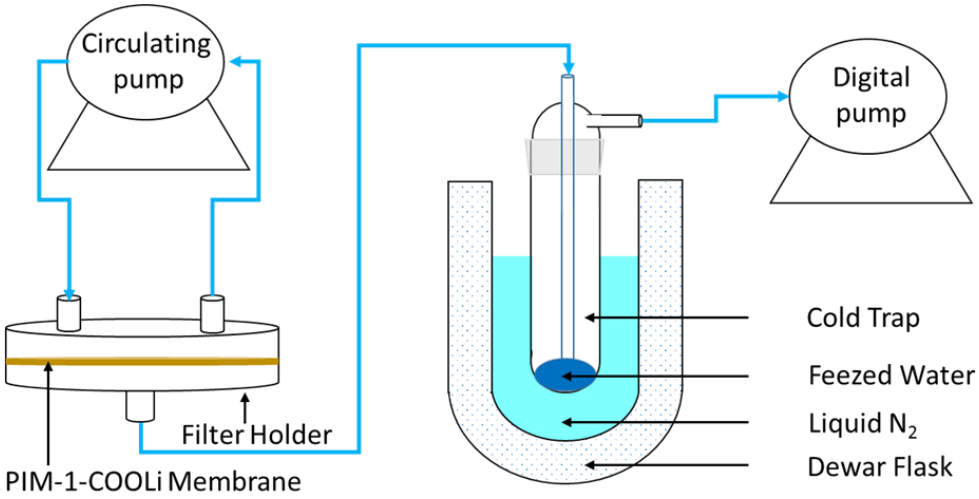

Fig. S7 Schematic illustration of the experimental set-up for the liquid permeation measurements.

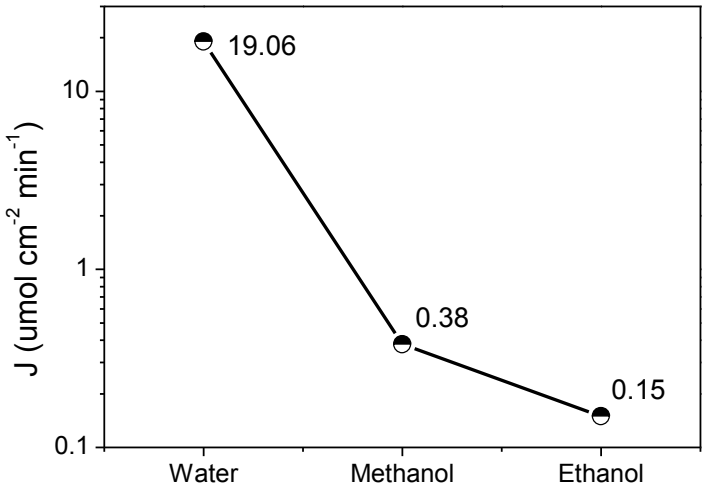

Fig. S8 The permeability of water, methanol and ethanol of the PIM-1-COOLi membrane measured at 25 ^{o}C and 10 Pa.

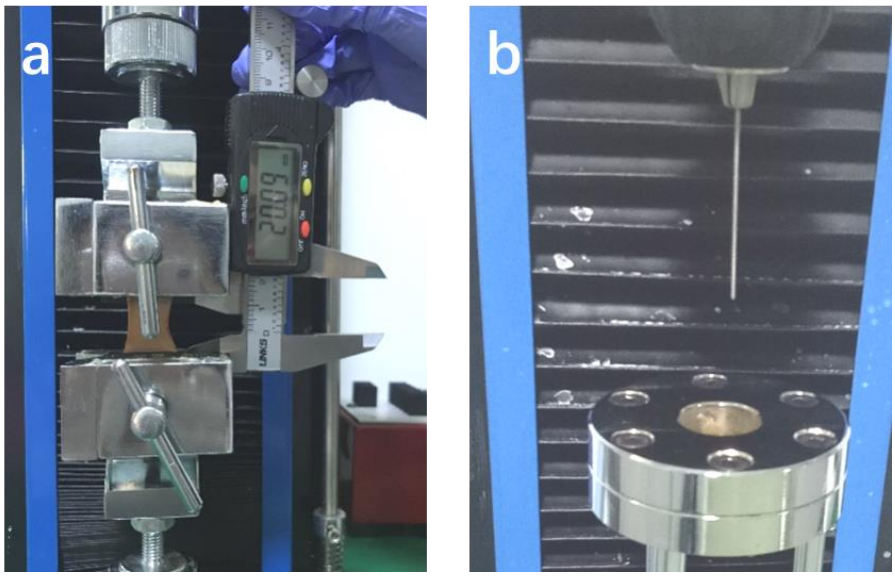

Fig. S9 The apparatus used for measuring the stretching (a) and punching (b) properties of the PIM-1-COOLi membrane.

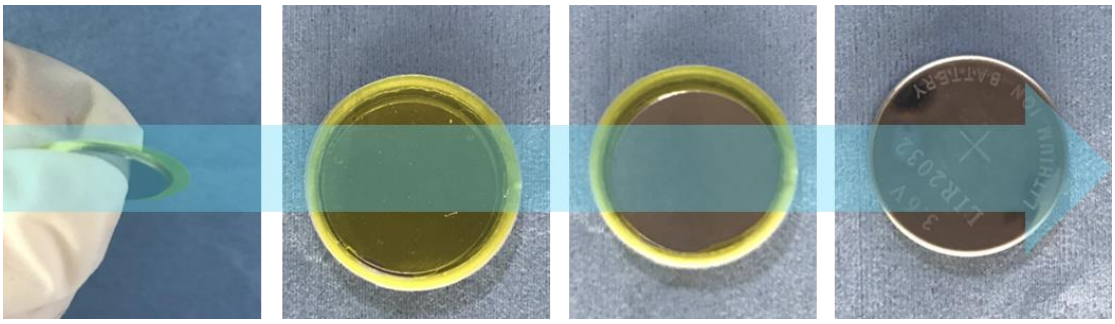

Fig. S10 The device assembly process used to measure the Li/Na ion conductivity of the membrane.

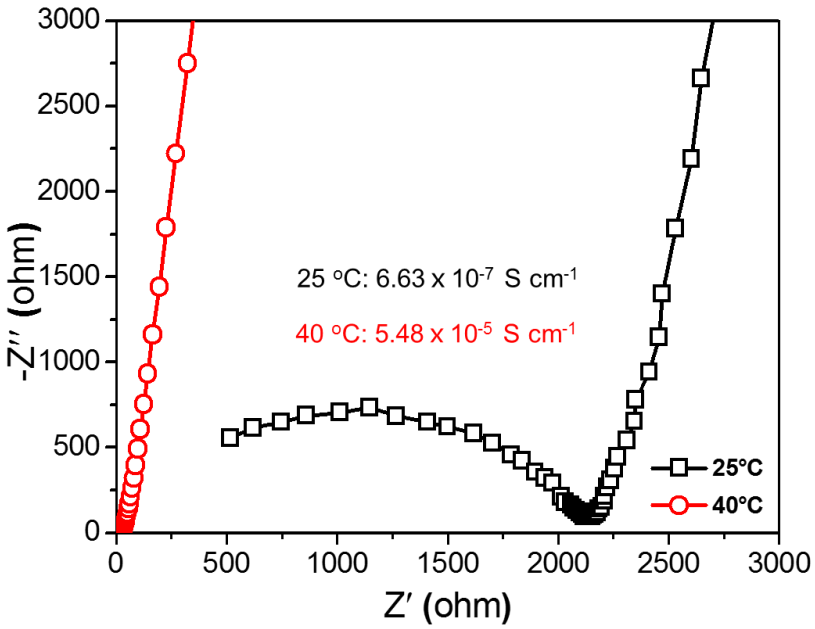

Fig. S11 The Nyquist plots in 0.1 M LiOH aqueous solution of PIM-1-COOLi membranes prepared at 25 °C and 40 °C for 24 h.

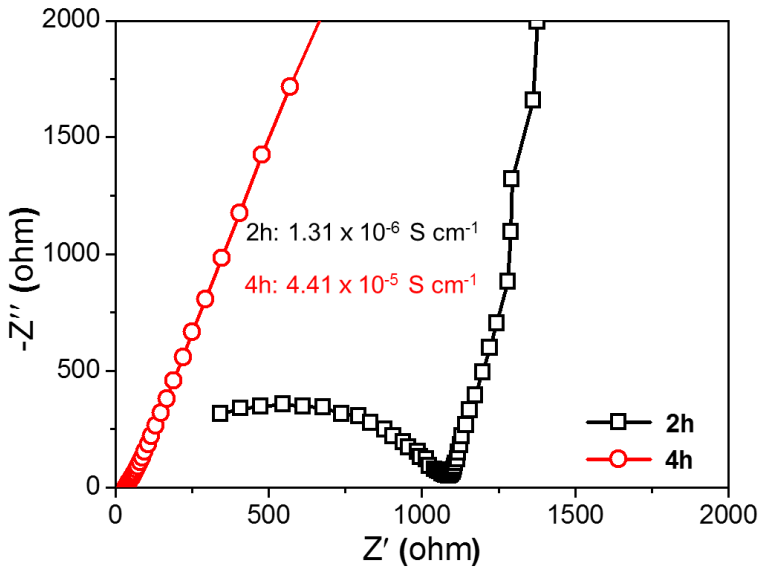

Fig. S12 The Nyquist plots in 0.1 M LiOH aqueous solution of PIM-1-COOLi membranes prepared at 60 °C for 2h and 4h.

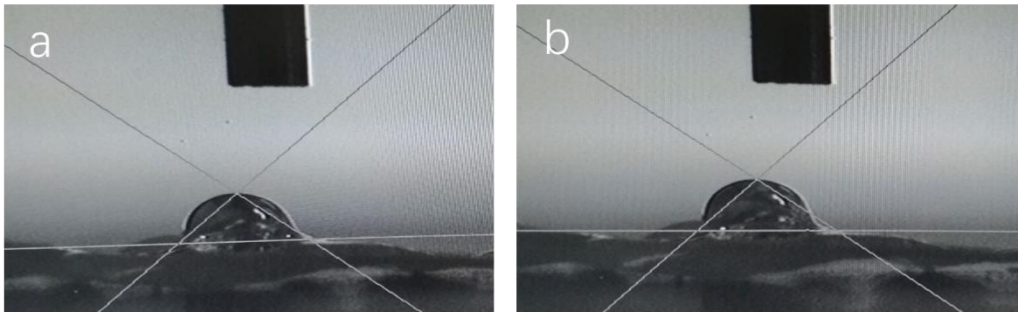

Fig. 13 Photo pictures showing the contact angles of EC/DEC (a) and water (b) drop on the PIM-1-COOLi membrane.

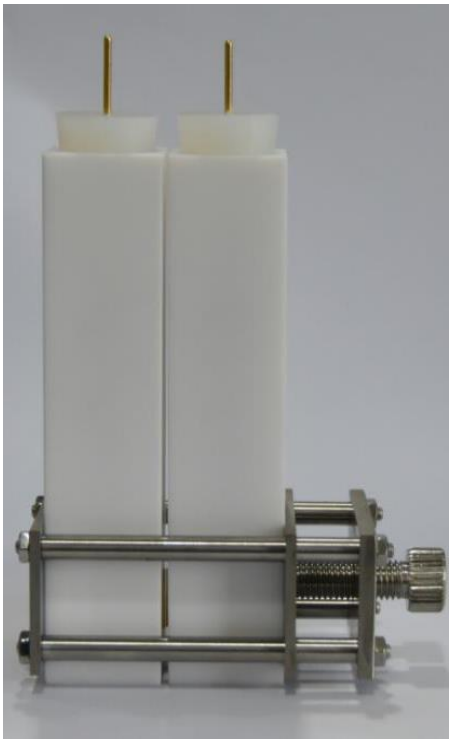

Fig. S14 Photo picture of an assembled metal-H_2O_2 hybrid-electrolytes mode cell.

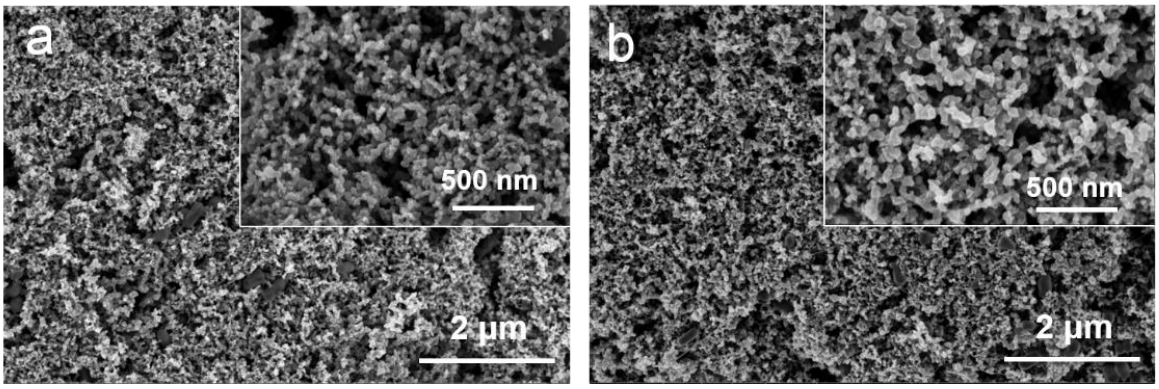

Fig. S15 SEM images of the cathode surface before (a) and after (b) battery discharging.

Table S1. Li^+ conductivity of typical polymer-based membranes.

	Li^+ Cond. (S cm^{-1})		**Ref**
Separator	**Aqu.**	**Org.**	
PEO		$4.06*10^{-7}$	RSC Adv., 2014, 4, 59637-59642
PP (Celgard 2400)	$1.34*10^{-3}$		J Mater Sci ,2014, 49:6961–6966
PEO/1%GO		$2*10^{-5}$	RSC Adv., 2014, 4, 59637-59642
N-PCPE		$5.7*10^{-4}$	Adv. Funct. Mater. 2014, 24, 44
PEO+LiTFSI+HNT		$1.11*10^{-4}$	Nano Energy, 2015, 16, 196
PAN- $LiClO_4$ -LLTO		$2.4*10^{-4}$	Nano Lett., 2015, 15 (4), 2740
SPE		$1.34*10^{-3}$	J. Power Sources, 2015, 284, 459
PEO/Li^+/PIL(TFSI)-FGbrush CPE		$7.9*10^{-5}$	J. Mater. Chem. A, 2015,3, 18064
PEG-αCD/PAA multilayer films		$2.5*10^{-5}$	Chem. Mater. 2016, 28, 2934
MB-PCPE		$1.03*10^{-3}$	Solid State Ionics 289 (2016) 1
PEO-LiTFSI-LGPS		$1.21*10^{-3}$ (80°C)	J. Power Sources 301 (2016) 47-53
PPC/LLZTO		$5.2*10^{-4}$	J. Mater. Chem. A, 2017,5, 4940
Bacterial cellulose	$3.27*10^{-3}$		Cellulose ,2017, 24:1889–1899
PVDF/Al_2O_3	$3.32*10^{-3}$		RSC Adv., 2017, 7, 24410
POSS-4PEG2K	$6.6*10^{-4}$		Adv. Energy Mater. 2017, 7, 1701231
PVDF-EC- (A-SiO2)/PE	$7.9*10^{-4}$		J. Power Sources, 2018, 407:44–52
$(M–P/P)_{10}$	$4.2*10^{-4}$		Adv. Energy Mater. 2018, 8, 1802430
PEO/CQDs NPEs		$1.39*10^{-4}$	Adv. Sci. 2018, 5, 1700996
PEO-NaTFSI-BMIMTFSI			J Solid State Electrochem, 2018. 22:1909.
PTFE-emimNTf2		$1.01*10^{-3}$	Adv. Energy Mater. 2018, 8, 1702702
SiO2-PAN@PAN-PU	$1.4*10^{-3}$		Electrochimica Acta, 2018, 292: 357-363
PVDF-HFP membranes modified by nano-ZnO	$1.4*10^{-3}$		Electrochimica Acta, 2018, 292: 769-778
Cellulose/styrene-co-acrylate composite (pCSA)	$1.34*10^{-3}$		Carbohydrate Polymers, 2019, 206:801–810
PVDF-HFP/PMIA	$1.21*10^{-3}$		Materials Letters, 2019, 236: 101–105
NGPEs	$8.9*10^{-3}$		J. Colloid Interface Sci., 2019 ,534: 672–682
SPEEK	0.033		Polym Int., 2019, 68: 120–124
PIM-1-COOLi	$6.5*10^{-3}$	$7.3*10^{-4}$	This work